ChemComm

ROYAL SOCIETY OF CHEMISTRY

COMMUNICATION

View Article Online
View Journal | View Issue

Cite this: *Chem. Commun.*, 2022, **58**, 7507

Received 10th May 2022,
Accepted 7th June 2022

DOI: 10.1039/d2cc02650c

rsc.li/chemcomm

A viologen-functionalized metal–organic framework for efficient CO_2 photoreduction reaction†

Tong Wang,[a] Lei Zhang,[b] Jiang Liu,*[ab] Xiao-Xin Li,[ac] Lin Yuan,[a] Shun-Li Li[b] and Ya-Qian Lan *[ab]

Here, a viologen-functionalized metal–organic framework (MOF), MIL-125-RV^{2+}, was obtained by modification of MIL-125-NH$_2$ with viologen molecules. MIL-125-RV^{2+}, the first viologen-based MOF for photocatalytic CO$_2$RR, exhibited excellent photocatalytic activity and high selectivity for HCOO$^-$. The strategy of using photo-responsive color-changing organics to functionalize the MOF is significant for achieving efficient CO$_2$RR.

With the development of sustainable carbon neutrality, the resourceful use of CO_2 has regained the attention of researchers.[1,2] The photocatalytic CO_2 reduction reaction (CO_2RR) is considered to be one of the most promising techniques, which uses renewable solar energy to reduce CO_2 to high value-added products.[3,4] Therefore, the development of wide absorption spectra, highly active CO_2RR photocatalysts is of great importance. Metal–organic frameworks (MOFs) are a class of hybrid materials consisting of metal ions/clusters linked to organic ligands. Owing to their rich catalytic sites and extremely open frameworks, MOFs have been widely used in photocatalysis.[5–7] Photoexcitation is a crucial step in photocatalytic reactions.[8] However, the band gaps of the majority of MOFs are usually wide (only responding to ultraviolet light), and they are unable to exploit the cleaner and milder power sources such as visible light.[9] In addition, the redox activity and electron transfer rate greatly limit the application of MOFs in photocatalysis.[10,11] Therefore, we are committed to finding a functionalized ligand that can ameliorate these disadvantages of MOFs, leading to more efficient photocatalytic CO_2 reduction.

A viologen derivative is a kind of photo-modulated color-changing material that undergoes two reversible reduction steps generating a radical cation (RV$^{\bullet+}$) and a neutral form (RV^0) under the stimulation of light. The radical electrons of RV$^{\bullet+}$ are delocalized in the large π-conjugated skeleton. Thus, the single electron (RV$^{\bullet+}$) state can remain stable and render intense coloring. This color change is accompanied by an increase in the spectral absorption range.[12] At the same time, viologen derivatives can serve as strong electron acceptors to exert outstanding electron transfer capability.[13–15] Based on the above advantages of viologen derivatives, combining viologen ligands with MOFs can be conducive to the application of MOFs as photocatalysts for photocatalytic CO_2RR. However, there are limited experimental studies of framework materials using viologen as a building block. Due to the weak affinity of the positively charged bipyridine molecules for metal ions, it is difficult to form coordination networks. The currently available viologen-based MOFs have long synthesis time and low yields, making them arduous to apply in practice. Hence, it is necessary to choose a straightforward method to construct viologen-based MOFs.

Based on the above considerations, a viologen-functionalized **MIL-125-RV^{2+}** was constructed by creatively using the Zincke reaction,[16] in which the viologen ligands (RV^{2+}) were modified on the stable skeleton of **MIL-125-NH$_2$**. Owing to the introduction of RV^{2+}, the migration of photogenerated charges in the skeleton is accelerated. And the light absorption range of **MIL-125-RV^{2+}** was extended from 550 to 670 nm. Accordingly, under 10 h visible light irradiation, the yield of HCOO$^-$ increased from 7.31 μmol to 12.13 μmol. In this work, the viologen derivative is covalently combined with framework materials, which is significant to explore distinctive advantages of viologen applied in photocatalytic CO_2RR.

With the robust and open skeleton of **MIL-125-NH$_2$**, the Zincke reaction of the amino group (–NH$_2$) of the ligand

[a] *Jiangsu Collaborative Innovation Centre of Biomedical Functional Materials, Jiangsu Key Laboratory of New Power Batteries, School of Chemistry and Materials Science, Nanjing Normal University, Nanjing 210023, P. R. China. E-mail: liuj@njnu.edu.cn, yqlan@m.scnu.edu.cn, yqlan@njnu.edu.cn, Web: https://www.yqlangroup.com*

[b] *School of Chemistry, South China Normal University, Guangzhou, 510006, P. R. China*

[c] *School of Chemistry and Chemical Engineering, Southeast University, Nanjing 211189, P. R. China*

† Electronic supplementary information (ESI) available. See DOI: **https://doi.org/10.1039/d2cc02650c**

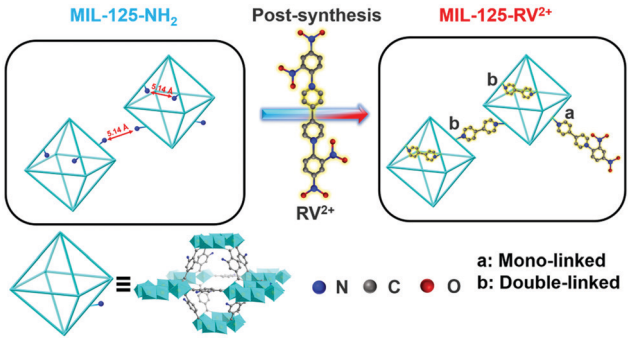

Scheme 1 Schematic representation of the design strategy for the construction of **MIL-125-RV^{2+}**.

(BDC-NH_2) with the RV^{2+} molecules was used to obtain the viologen-functionalized **MIL-125-RV^{2+}** (Scheme 1). To verify the anchoring of RV^{2+} in **MIL-125-RV^{2+}**, the two materials were tested by Fourier transform infrared spectroscopy (FTIR) (Fig. 1a). The spectra show that the typical peaks (3446, 3353 and 1659 cm^{-1}) attributed to $-NH_2$ are significantly weakened after the modification with RV^{2+} molecules.[17–19] Meanwhile, the new peak at around 3050 cm^{-1} belongs to the C–H bond of the pyridine ring.[20] Notably, the characteristic peak of C–NO_2 appears at 840 cm^{-1}. This suggests that the majority RV^{2+} molecules in the final **MIL-125-RV^{2+}** are mono-linked. This result is confirmed by the high-resolution N 1s X-ray photoelectron spectroscopy (XPS) spectra. The new peak at 406.3 eV indicates the presence of O═N═O (Fig. 1b). Meanwhile, as shown in Scheme 1, a bipyridine molecule can also be anchored to two adjacent $-NH_2$. This circumstance is referred to as double-linked.

Powder X-ray diffraction (PXRD) patterns of the obtained **MIL-125-RV^{2+}** corresponded well with the measured **MIL-125-NH$_2$**

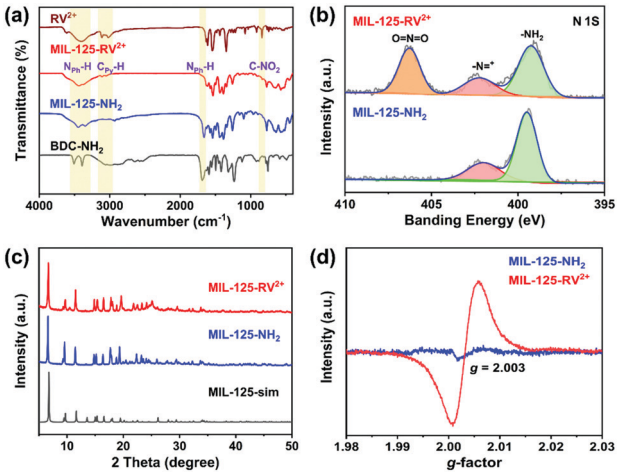

Fig. 1 Structural characterizations. (a) FT-IR spectra of RV^{2+} ligands, **MIL-125-NH$_2$**, **MIL-125-RV^{2+}**and BDC-NH_2 ligands. (b) The high-resolution N 1s XPS spectra of **MIL-125-NH$_2$** and **MIL-125-RV^{2+}**. (c) PXRD patterns of measured **MIL-125-NH$_2$**, **MIL-125-RV^{2+}** and the simulated MIL-125. (d) EPR spectra of **MIL-125-NH$_2$** and **MIL-125-RV^{2+}** under visible-light irradiation.

(Fig. 1c), which proves the non-destructive transformation of the framework.[21] Afterward, the modified **MIL-125-RV^{2+}** was digested with HF (30%) and DMSO-d_6, and the obtained solution was analyzed by ^{1}H-NMR (Nuclear Magnetic Resonance) to evaluate the percentage of post-synthetic conversion. Approximately 24% of the BDC-NH_2 linkers were reacted with RV^{2+} molecules (Fig. S7, ESI†). When an RV^{2+} molecule accepts an electron, it leads to the formation of a cationic radical ($RV^{\bullet+}$). The unique redox ability of **MIL-125-RV^{2+}** was verified by electron paramagnetic resonance (EPR). Under 300 W Xe lamp (>420 nm) irradiation, **MIL-125-RV^{2+}** exhibits a strong EPR peak centered at g = 2.003, which is attributed to the signal of $RV^{\bullet+}$, and there is no such peak in the spectrum of **MIL-125-NH$_2$** (Fig. 1d). This result not only indicates the presence of bipyridine functional units in **MIL-125-RV^{2+}**, but also confirms that **MIL-125-RV^{2+}** undergoes a rapid single electron transfer under light excitation (Fig. S10, ESI†). Moreover, the characteristic redox of **MIL-125-RV^{2+}** was revealed *via* cyclic voltammetry (CV) profiles (Fig. S11, ESI†). **MIL-125-RV^{2+}** shows two reversible single-electron reductions due to the distinctive redox of viologen. The reduction potential of **MIL-125-RV^{2+}** (E_{red1} = −0.38 V *vs.* Ag/AgCl) is much higher than that of **MIL-125-NH$_2$** (E_{red} = −1.11 V *vs.* Ag/AgCl), showing the stronger electron-accepting ability.[20] Thus, the introduction of the RV^{2+} functional group effectively enhances the redox activity of **MIL-125-RV^{2+}**.

To reveal the effect of viologen functional groups on the light absorption capacity of **MIL-125-RV^{2+}**, a UV-vis diffuse reflectance spectroscopy (UV-vis DRS) test was carried out. Compared with the original **MIL-125-NH$_2$**, **MIL-125-RV^{2+}** shows further elevated absorption in the visible light region. The enhancement of light absorption can be associated with the presence of $RV^{\bullet+}$. This change in absorption is accompanied by a decrease in the gap energy.[22,23] The optical band gap (E_g) of **MIL-125-NH$_2$** and **MIL-125-RV^{2+}** was calculated to be 2.47 eV and 2.14 eV by Tauc plots (Fig. 2b). The Mott–Schottky plots were used to determine the LUMO levels of both materials (Fig. 2c and Fig. S12, ESI†). The corresponding values were evaluated to be −0.85 (**MIL-125-NH$_2$**) and −1.08 V (**MIL-125-RV^{2+}**) (*vs.* NHE, pH = 7). Based on the data of the band gaps and Mott–Schottky plots, the band structure diagrams of **MIL-125-NH$_2$** and **MIL-125-RV^{2+}** were obtained (Fig. 2d). This demonstrates that **MIL-125-RV^{2+}** can be used as a photocatalyst for the CO_2RR theoretically.[24]

The photocatalytic tests were performed under visible irradiation (λ > 420 nm) in a mixed solvent [acetonitrile and triethanolamine (TEOA)] without any photosensitizers and noble metal co-photocatalysts. Under 10 hours of visible-light irradiation, the yield of $HCOO^-$ for **MIL-125-NH$_2$** is 7.31 μmol, which is generally consistent with previous reports.[21] When **MIL-125-RV^{2+}** was used as a photocatalyst, the yield of $HCOO^-$ rose to 12.13 μmol, which is 1.6 times the catalytic activity of the original **MIL-125-NH$_2$**. Gas chromatography (GC) showed no gas-phase products, and H_2 as a competitive product was not detected during the reaction, suggesting that the selectivity of **MIL-125-RV^{2+}** was not decreased after the modification of RV^{2+} (Fig. S12, ESI†). What's more, the apparent quantum efficiency (AQE) for $HCOO^-$ evolution was measured under

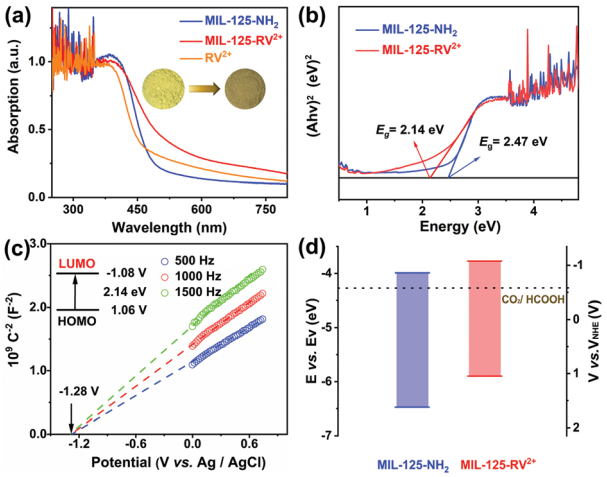

Fig. 2 Optical characterizations. (a) UV-vis DRS of the RV^{2+} ligand, **MIL-125-NH$_2$** and **MIL-125-RV^{2+}**. Inset: Photographs of **MIL-125-NH$_2$** and **MIL-125-RV^{2+}**. (b) Band gap energy (E_g) analysis. (c) Mott–Schottky plots for **MIL-125-RV^{2+}** in 0.5 M Na_2SO_4 aqueous solution. Inset: The energy diagram of the HOMO and LUMO levels of **MIL-125-RV^{2+}**. (d) Energy bandgap diagrams of **MIL-125-NH$_2$** and **MIL-125-RV^{2+}** with respect to the CO_2RR potentials (pH = 7).

monochromatic light (420/450/500 nm). The result means that the AQE of **MIL-125-RV^{2+}** is relatively higher compared to **MIL-125-NH$_2$** (Table S2, ESI†), which reveals that the existence of viologen compounds improves the light utilization of the photocatalyst. Then, the photocatalytic stability was evaluated by recycling experiments (Fig. 3b). **MIL-125-RV^{2+}** retained at least 95% of its original activity after four cycles. The recovered photocatalysts were characterized by PXRD, FTIR, UV-vis DRS and ^{1}H NMR (Fig. S14–S17, ESI†). All the data reveal that

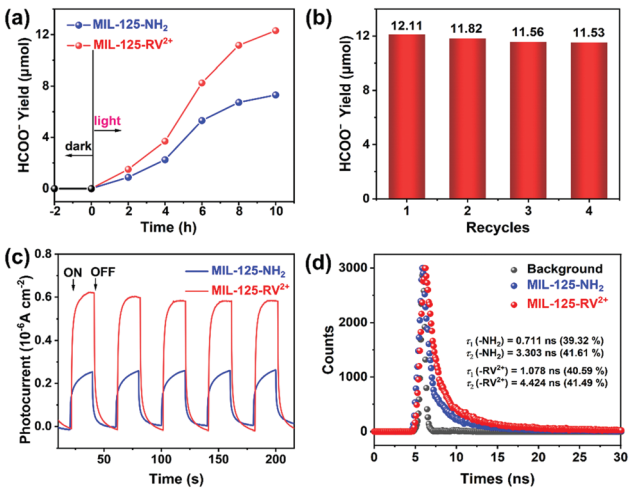

Fig. 3 Photocatalytic performance and electron transfer properties. (a) Time-dependent $HCOO^-$ yield of **MIL-125-NH$_2$** and **MIL-125-RV^{2+}**. (b) Yield of $HCOO^-$ for **MIL-125-RV^{2+}** as a CO_2RR photocatalyst in four continuous runs. (c) Transient photocurrent responses of **MIL-125-NH$_2$** and **MIL-125-RV^{2+}** under visible-light irradiation. (d) Time-resolved PL spectra of **MIL-125-NH$_2$** and **MIL-125-RV^{2+}**.

viologen ligands of **MIL-125-RV^{2+}** were not altered after the catalytic cycles.

Subsequently, a series of careful controlled experiments were carried out without light irradiation, photocatalyst or CO_2 (replaced by Ar). The results showed that IC and GC did not detect any product. It is evident that the entire CO_2RR is driven by light irradiation and **MIL-125-RV^{2+}** acts as a photocatalyst for the reaction. Notably, when the physical mixture of **MIL-125-NH$_2$** and RV^{2+} ligands was used as a photocatalyst, the RV^{2+} molecules dissolved under the photoreaction conditions, and the yield of $HCOO^-$ was only 4.53 μmol, which reflects the advantage of the covalent connection between the RV^{2+} ligands and MOF skeleton. Importantly, the carbon source of $HCOO^-$ was confirmed to be CO_2 by the isotopic $^{13}CO_2$ experiment under the same catalytic conditions. The ^{13}C NMR spectrum gave a clear signal at 162.6 ppm, which is consistent with the standard signal for $HCOO^-$ in the literature (Fig. S18 and S19, ESI†).[25]

To figure out the reasons for the enhanced photocatalytic activity of **MIL-125-RV^{2+}**, the electronic properties of both photocatalysts were investigated. The transient photocurrent (TPC) response test can intuitively reflect the efficiency of photocatalyst photogenerated charge separation and migration. Under periodic illumination, both **MIL-125-NH$_2$** and **MIL-125-RV^{2+}** exhibited a sharp and stable photocurrent response. The stronger response of **MIL-125-RV^{2+}** than **MIL-125-NH$_2$** is well-matched with their photocatalytic performance. Moreover, the much lower electrochemical impedance of **MIL-125-RV^{2+}** than that of **MIL-125-NH$_2$** determined by Nyquist plots can facilitate photogenerated charge migration to the catalyst surface (Fig. S19, ESI†). Since the structures of **MIL-125-NH$_2$** and **MIL-125-RV^{2+}** are essentially identical, the accelerated migration of photogenerated charges in the skeleton can be attributed to the presence of RV^{2+} ligands. Correspondingly, the time-resolved photoluminescence (PL) spectra showed that the fluorescence lifetime of **MIL-125-RV^{2+}** was significantly longer than that of **MIL-125-NH$_2$**, indicating that the grafting of RV^{2+} on **MIL-125-RV^{2+}** can effectively inhibit charge recombination and prolong the lifetime of charge carries (Fig. 3d).[26] It is also confirmed by the fluorescence quenching of **MIL-125-RV^{2+}** in the steady-state PL spectra (Fig. S21, ESI†).

The vital intermediates from CO_2 to $HCOO^-$ were monitored by *in situ* Fourier transform infrared (FTIR) spectroscopy (Fig. 4a). The peak at 1716 cm^{-1} is attributed to $CO_2^{\bullet-}$, which is considered as one of the essential intermediates of CO_2 $HCOO^-$.[26] Besides, the formation of carboxylate (COO^-) is confirmed by the peak at 1266, 1521, 1539, and 1556 cm^{-1}.[27–30] Thereafter, the intermediate (COO^-) underwent a step of hydrogenation to be $HCOO^-$ (1384 cm^{-1}).[31] Combining previous studies with the above data analysis, a plausible mechanism is proposed to explain the photocatalytic CO_2RR of **MIL-125-RV^{2+}** (Fig. 4b).[21,32] To begin with, under the light harvesting of RV^{2+} ligands, a large number of electron-hole pairs are generated of **MIL-125-RV^{2+}**. Ti^{4+} ions in the titanium oxo-clusters acquire the photoexcited electrons migrated from the ligands to become Ti^{3+} ions. The charge

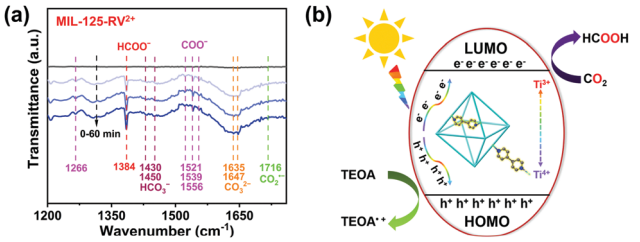

Fig. 4 Mechanism illustration. (a) *In situ* FTIR spectra on **MIL-125-RV^{2+}**. (b) Plausible mechanism for photocatalytic CO_2RR over **MIL-125-RV^{2+}** under visible-light irradiation.

migration in this process is accelerated by the introduction of the RV^{2+} ligands. Subsequently, the excited electrons move further toward the adsorbed CO_2 molecules for the CO_2RR, while the Ti^{3+} ions are oxidized to the original Ti^{4+} ions. TEOA acts as sacrificial agent to be oxidized by photogenerated holes. Therefore, a complete photocycle of CO_2 to $HCOO^-$ can be achieved by **MIL-125-RV^{2+}** with the presence of CO_2 and TEOA.

In summary, a viologen-functionalized MOF photocatalyst (**MIL-125-RV^{2+}**) was successfully constructed by a straightforward post-synthetic method and for the first time applied to photocatalytic CO_2RR. The light absorption of **MIL-125-RV^{2+}** is enhanced compared to **MIL-125-NH$_2$**. TPC, EIS and PL tests indicate that the introduction of viologen as functional units is favourable to accelerate the migration rate of photogenerated charges in the skeleton of MOFs, thus optimizing the photocatalytic performance of the CO_2RR. Under visible-light irradiation, the photocatalytic activity of **MIL-125-RV^{2+}** can reach 1.6 times that of **MIL-125-NH$_2$** under the same conditions. Significantly, photo-modulated color-changing organics were used to functionalise MOFs in this work. It is expected that these results will boost the design and development of photocatalysts for the CO_2RR based on MOF materials.

This work was financially supported by NSFC (No. 92061101, 21871141, 21871142 and 22071109); the Excellent Youth Foundation of NSF of Jiangsu Province (No. BK20211593); the Guangdong Basic and Applied Basic Research Foundation (No. 2021A1515110429); the Priority Academic Program Development of Jiangsu Higher Education Institutions and the Foundation of Jiangsu Collaborative Innovation Center of Biomedical Functional Materials.

Conflicts of interest

There are no conflicts to declare.

Notes and references

1 H. L. van Soest, M. G. J. den Elzen and D. P. van Vuuren, *Nat. Commun.*, 2021, **12**, 2140.
2 M. He, Y. Sun and B. Han, *Angew. Chem., Int. Ed.*, 2013, **52**, 9620–9633.
3 X. Chang, T. Wang and J. Gong, *Energy Environ. Sci.*, 2016, **9**, 2177–2196.
4 J. Li, H. Huang, W. Xue, K. Sun, X. Song, C. Wu, L. Nie, Y. Li, C. Liu, Y. Pan, H.-L. Jiang, D. Mei and C. Zhong, *Nat. Catal.*, 2021, **4**, 719–729.
5 Y. Qin, M. Hao, D. Wang and Z. Li, *Dalton Trans.*, 2021, **50**, 13201–13215.
6 D. Y. Lee, I. Lim, C. Y. Shin, S. A. Patil, W. Lee, N. K. Shrestha, J. K. Lee and S.-H. Han, *J. Mater. Chem. A*, 2015, **3**, 22669–22676.
7 D. Y. Ahn, D. Y. Lee, C. Y. Shin, H. T. Bui, N. K. Shrestha, L. Giebeler, Y.-Y. Noh and S.-H. Han, *ACS Appl. Mater. Interfaces*, 2017, **9**, 12930–12935.
8 Y. Jiao, L. Đorđević, H. Mao, R. M. Young, T. Jaynes, H. Chen, Y. Qiu, K. Cai, L. Zhang, X.-Y. Chen, Y. Feng, M. R. Wasielewski, S. I. Stupp and J. F. Stoddart, *J. Am. Chem. Soc.*, 2021, **143**, 8000–8010.
9 H. Khajavi, J. Gascon, J. M. Schins, L. D. A. Siebbeles and F. Kapteijn, *J. Phys. Chem. C*, 2011, **115**, 12487–12493.
10 X. Zhou and H. Dong, *ChemCatChem*, 2019, **11**, 3688–3715.
11 X. Ma, H. Liu, W. Yang, G. Mao, L. Zheng and H.-L. Jiang, *J. Am. Chem. Soc.*, 2021, **143**, 12220–12229.
12 B. L. Feringa, R. A. van Delden, N. Koumura and E. M. Geertsema, *Chem. Rev.*, 2000, **100**, 1789–1816.
13 G. Li, B. Zhang, J. Wang, H. Zhao, W. Ma, L. Xu, W. Zhang, K. Zhou, Y. Du and G. He, *Angew. Chem., Int. Ed.*, 2019, **58**, 8468–8473.
14 J. Ding, C. Zheng, L. Wang, C. Lu, B. Zhang, Y. Chen, M. Li, G. Zhai and X. Zhuang, *J. Mater. Chem. A*, 2019, **7**, 23337–23360.
15 G. Huseynova, N. K. Shrestha, Y. Xu, E.-Y. Shin, W.-T. Park, D. Ji and Y.-Y. Noh, *Org. Electron.*, 2018, **62**, 572–580.
16 D. Barbier, C. Marazano, C. Riche, B. C. Das and P. Potier, *J. Org. Chem.*, 1998, **63**, 1767–1772.
17 D. Dai, J. Qiu, L. Zhang, H. Ma and J. Yao, *J. Colloid Interface Sci.*, 2022, **607**, 933–941.
18 X. Chen, Y. Kondo, S. Li, Y. Kuwahara, K. Mori, D. Zhang, C. Louis and H. Yamashita, *J. Mater. Chem. A*, 2021, **9**, 26371–26380.
19 X. Huang, X. Li, Q. Luan, K. Zhang, Z. Wu, B. Li, Z. Xi, W. Dong and G. Wang, *Nano Res.*, 2021, **14**, 4250–4257.
20 Z. Mi, T. Zhou, W. Weng, J. Unruangsri, K. Hu, W. Yang, C. Wang, K. A. I. Zhang and J. Guo, *Angew. Chem., Int. Ed.*, 2021, **60**, 9642–9649.
21 Y. Fu, D. Sun, Y. Chen, R. Huang, Z. Ding, X. Fu and Z. Li, *Angew. Chem., Int. Ed.*, 2012, **51**, 3364–3367.
22 L. Zhang, P. Cui, H. Yang, J. Chen, F. Xiao, Y. Guo, Y. Liu, W. Zhang, F. Huo and B. Liu, *Adv. Sci.*, 2016, **3**, 1500243.
23 N. Afzali, S. Tangestaninejad, R. Keshavarzi, V. Mirkhani, J. Nematollahi, M. Moghadam, I. Mohammadpoor-Baltork, M. Reimer, S. Olthof, A. Klein and S. Gimenez, *ACS Sustainable Chem. Eng.*, 2020, **8**, 18366–18376.
24 H.-Q. Xu, J. Hu, D. Wang, Z. Li, Q. Zhang, Y. Luo, S.-H. Yu and H.-L. Jiang, *J. Am. Chem. Soc.*, 2015, **137**, 13440–13443.
25 N. R. Babij, E. O. McCusker, G. T. Whiteker, B. Canturk, N. Choy, L. C. Creemer, C. V. D. Amicis, N. M. Hewlett, P. L. Johnson, J. A. Knobelsdorf, F. Li, B. A. Lorsbach, B. M. Nugent, S. J. Ryan, M. R. Smith and Q. Yang, *Org. Process Res. Dev.*, 2016, **20**, 661–667.
26 J.-J. Liu, N. Li, J.-W. Sun, J. Liu, L.-Z. Dong, S.-J. Yao, L. Zhang, Z.-F. Xin, J.-W. Shi, J.-X. Wang, S.-L. Li and Y.-Q. Lan, *ACS Catal.*, 2021, **11**, 4510–4519.
27 X.-X. Li, L. Zhang, L. Yuan, T. Wang, L.-Z. Dong, K. Huang, J. Liu and Y.-Q. Lan, *Chem. Eng. J.*, 2022, **442**, 136157.
28 S. Gong, G. Zhu, R. Wang, F. Rao, X. Shi, J. Gao, Y. Huang, C. He and M. Hojamberdiev, *Appl. Catal., B*, 2021, **297**, 120413.
29 L. Wang, E. Guan, Y. Wang, L. Wang, Z. Gong, Y. Cui, X. Meng, B. C. Gates and F.-S. Xiao, *Nat. Commun.*, 2020, **11**, 1033.
30 X. Zu, X. Li, W. Liu, Y. Sun, J. Xu, T. Yao, W. Yan, S. Gao, C. Wang, S. Wei and Y. Xie, *Adv. Mater.*, 2019, **31**, 1808135.
31 Z. Wu, H. Wu, W. Cai, Z. Wen, B. Jia, L. Wang, W. Jin and T. Ma, *Angew. Chem., Int. Ed.*, 2021, **60**, 12554–12559.
32 Z. Jiang, J. Liu, M. Gao, X. Fan, L. Zhang and J. Zhang, *Adv. Mater.*, 2017, **29**, 1603369.

